SUPPORTING INFORMATION

Assessing Nickel Oxide Electrocatalysts Incorporating Diamines and Having Improved Oxygen Evolution Activity Using Operando UV/visible and X-ray Absorption Spectroscopy

Takafumi Miura,[a,†] Shun Tsunekawa,[a,†] Sho Onishi,[b] Toshiaki Ina,[c] Kehsuan Wang,[d] Genta Watanabe,[d] Chechia Hu,[e] Hiroshi Kondoh,[b] Takeshi Kawai,[d] and Masaaki Yoshida[*,a,f,g]

[a] *Yamaguchi University, Tokiwadai, Ube, Yamaguchi 755-8611, Japan*

[b] *Keio University, Hiyoshi, Kohoku-ku, Yokohama, Kanagawa 223-8522, Japan*

[c] *Japan Synchrotron Radiation Research Institute (JASRI), Sayo, Hyogo 679-5198, Japan*

[d] *Tokyo University of Science, Kagurazaka, Shinjuku-ku, Tokyo 162-8601, Japan*

[e] *National Taiwan University of Science and Technology, Taipei 10607, Taiwan*

[f] *ICAT Fellow, Institute for Catalysis, Hokkaido University, Japan*

[g] *Blue Energy Center for SGE Technology (BEST), Yamaguchi University, Japan*

[†]These authors contributed equally.

E-mail: yoshida3@yamaguchi-u.ac.jp

Index

i) The effect of the electrodeposition current on the OER current of the EDA catalyst

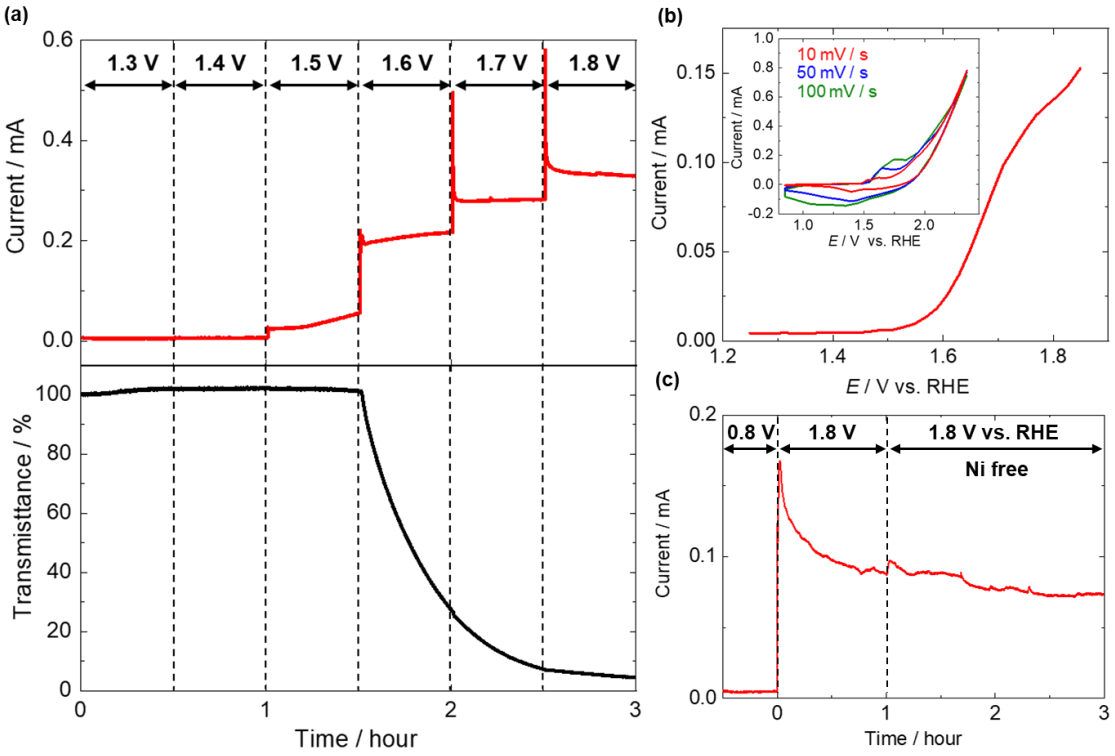

Figure S1. (a) Step scan data showing oxidation currents and transmittance values at 420 nm from UV/visible absorption during the electrodeposition of the Ni-EDA catalyst on an ITO substrate in a pH 11 K−P_i buffer containing $Ni(NO_3)_2$ and EDA. This figure demonstrates that the electrodeposition proceeded at electrode potentials greater than 1.6 V vs. RHE. (b) Linear sweep voltammogram and cyclic voltammogram (inset) obtained from the EDA catalyst on the ITO substrate in a pH 11 K−P_i buffer, indicating that the OER proceeded at electrode potentials over 1.5 V vs. RHE. (c) Time course of the OER current generated by the EDA catalyst on the ITO electrode at 1.8 V vs. RHE after changing the electrolyte solution from a pH 11 K−P_i buffer containing $Ni(NO_3)_2$ and EDA to one not containing these compounds. The oxidation currents were almost equivalent in both buffers, suggesting that the oxidation current associated with electrodeposition was sufficiently small compared with that of the OER.

ii) TEM image and XRD pattern

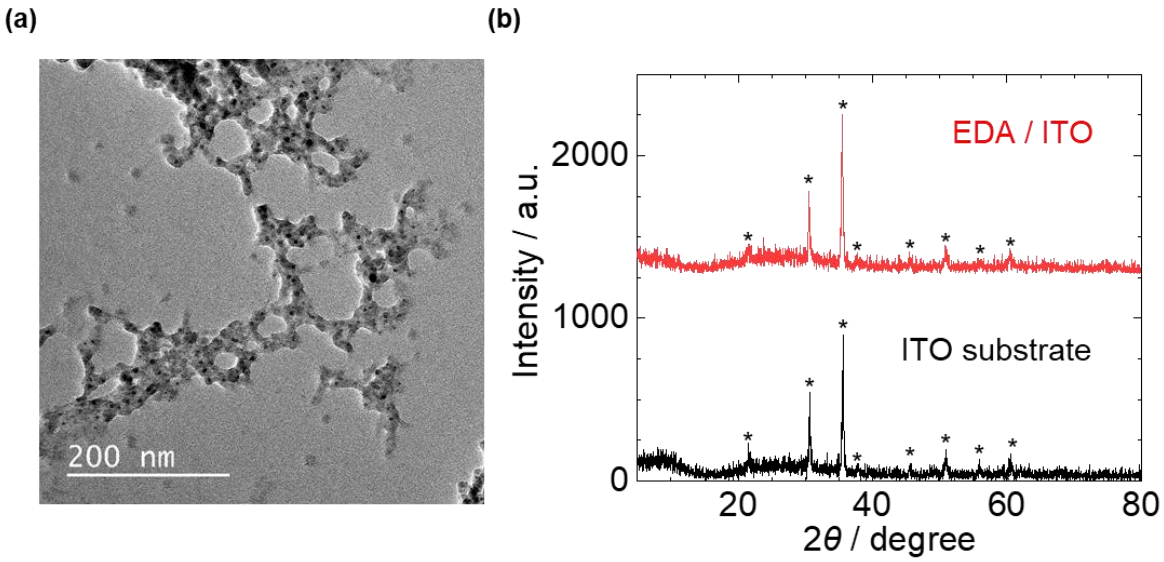

Figure S2. (a) TEM image and (b) XRD pattern obtained from an EDA catalyst on an ITO substrate after a 1 h electrodeposition at 1.8 V vs. RHE in a pH 11 K−P_i buffer containing $Ni(NO_3)_2$ and EDA. These results confirm that the EDA catalyst was composed of clusters having sizes of several hundred nm with an amorphous structure. Note that the EDA catalyst was peeled off the ITO substrate using Milli-Q water and transferred to a Au mesh holder prior to acquiring the TEM image.

iii) XPS spectra

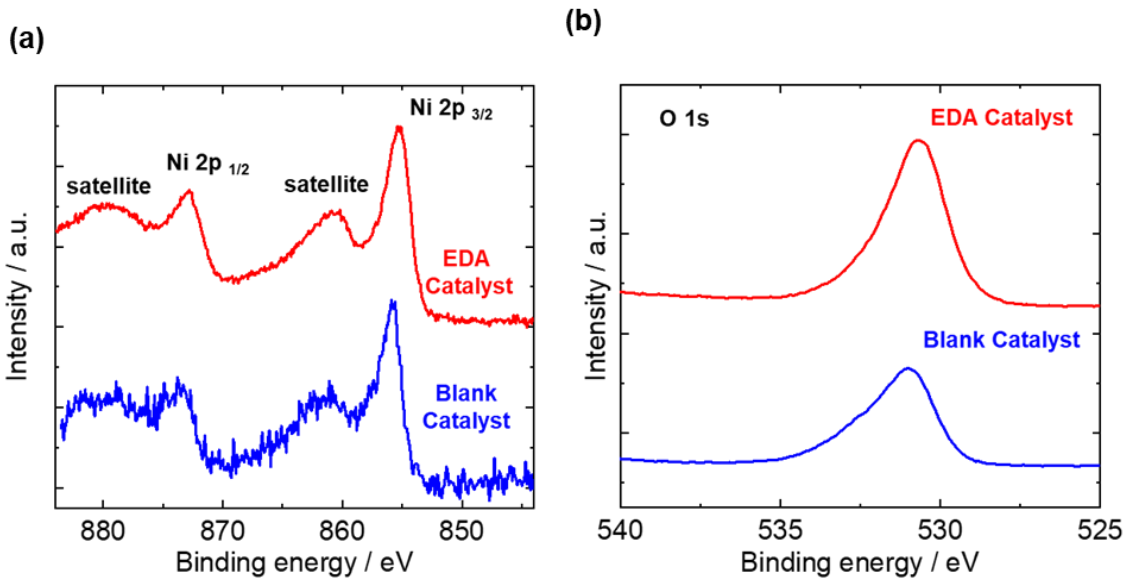

Figure S3. (a) Ni 2p and (b) O 1s XPS spectra obtained from the EDA and Blank catalysts. The presence of Ni and O species was confirmed in both the EDA and Blank catalysts. Note that the chemical states and local structures were also investigated in detail using XAFS, as shown in Figure 7.

iv) Stability of EDA Ni catalyst

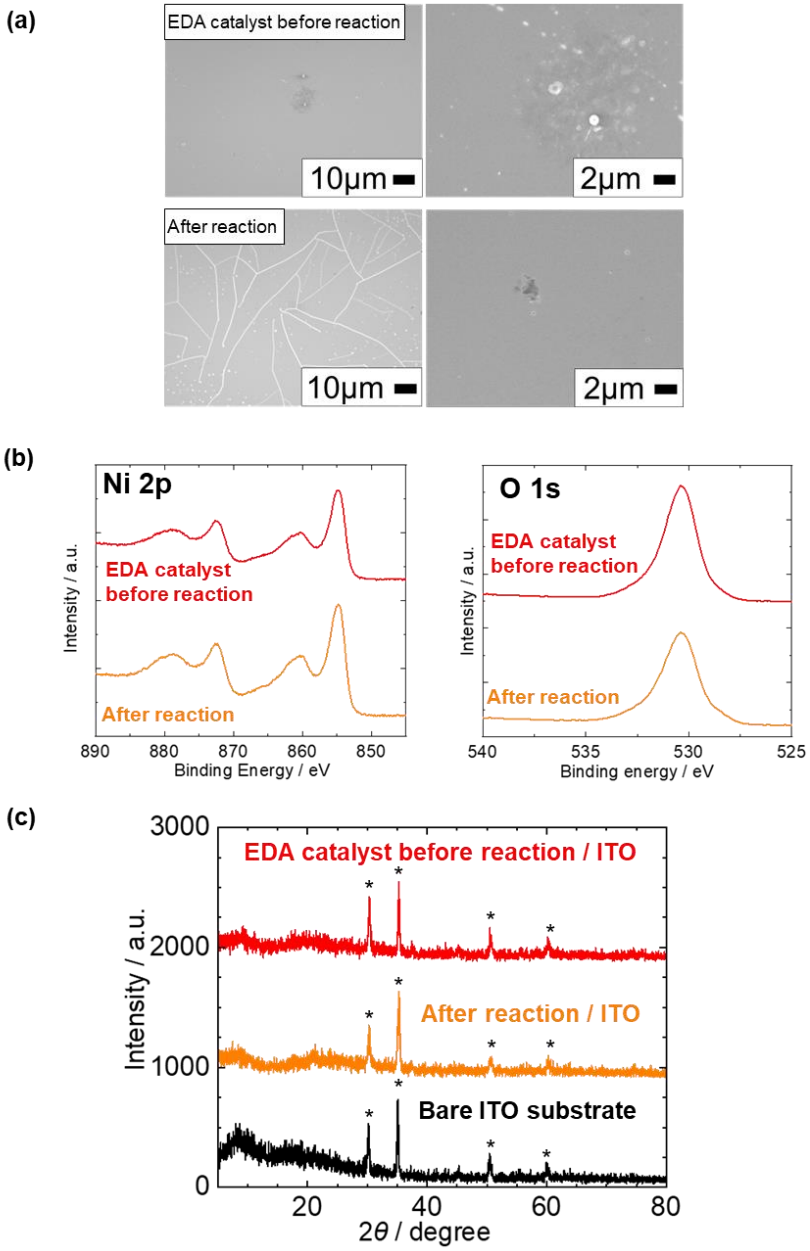

Figure S4. (a) SEM images, (b) XPS spectra, and (c) XRD patterns for EDA Ni catalyst before and after OER reaction. These results indicated that the images and spectra were almost the same between catalyst before and after OER reaction, suggesting that the EDA Ni catalysts can stably function as an efficient OER catalyst.

v) Characterization of Ni complexes with linear diamine molecules

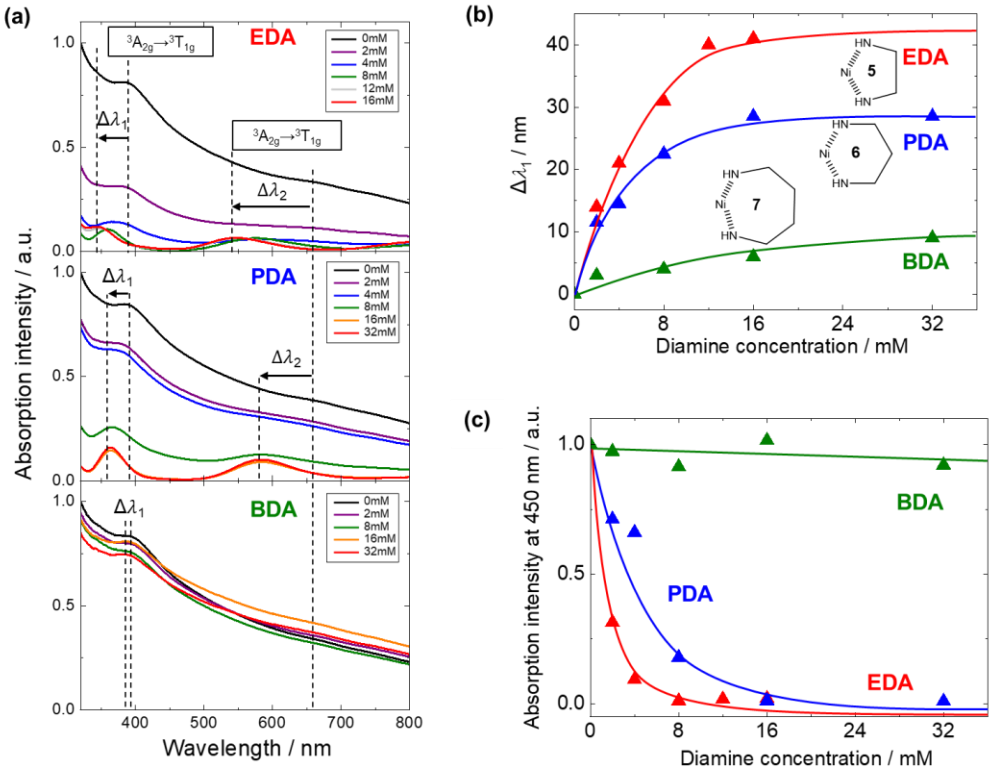

Figure S5. (a) UV/vis spectra of pH 11 0.1 M K−P_i buffers containing 4 mM $Ni(NO_3)_2$ and diamines with different carbon chain lengths (1,2-ethylenediamine (EDA), 1,3-propanediamine (PDA) and 1,4-butanediamine (BDA)) at varying concentrations. Gradual absorption was observed over the entire UV/vis regions as large background in the spectra, because the incident UV/vis beams were scattered by the generation of insoluble Ni colloids. When the diamine molecules were added in the solution, the background intensity dramatically decreased in the entire regions, indicating that the Ni colloids dissolved in the solution by formation of Ni complex with diamine molecules. The (b) peak shift ($\Delta\lambda_1$) and (c) absorption intensity at 450 nm estimated from the UV/vis spectra as functions of the diamine concentration. A larger $\Delta\lambda_1$ and decreased absorption intensity indicate the formation of Ni^{2+} complexes with the diamines and the dissolution of colloidal particles in the solution, respectively. Therefore, these results demonstrate that the formation of complexes of 5-membered ring (EDA) and 6-membered ring (PDA) compounds proceeded more efficiently compared with that of a 7-membered ring (BDA).

vi) Characterization of Ni complexes with methylated diamine molecules

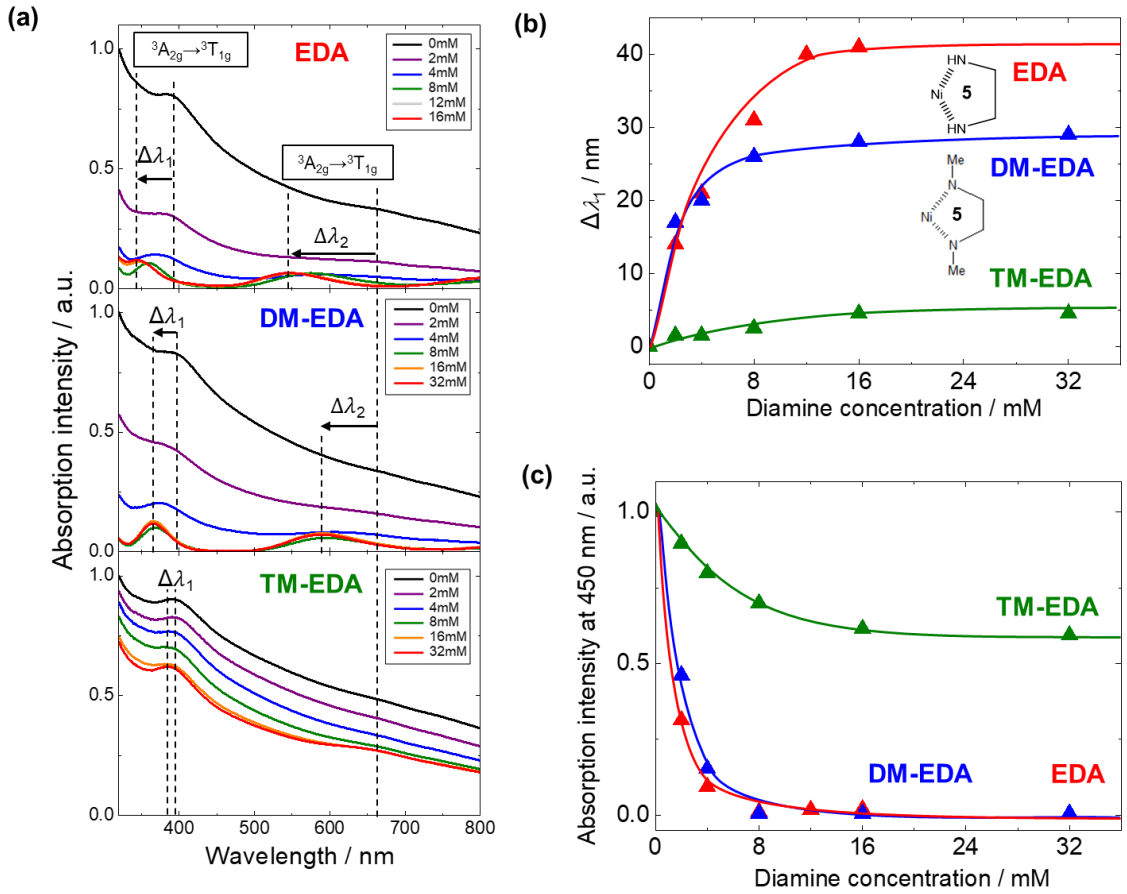

Figure S6. (a) The UV/vis spectra of pH 11 0.1 M K−P_i buffers containing 4 mM $Ni(NO_3)_2$ and diamine or methylated diamine molecules (1,2-ethylenediamine (EDA), *N*,*N*′-dimethylethylenediamine (DM-EDA) and *N*,*N*,*N*′,*N*′-tetramethylethylenediamine (TM-EDA)) at varying concentrations. Gradual absorption peaks were observed over the entire regions in the spectra because of the formation of insoluble colloids. The (b) peak shift ($\Delta\lambda_1$) and (c) absorption intensity at 450 nm estimated from the UV/vis spectra as functions of the diamine concentration. As described in the caption to Figure S5, a larger $\Delta\lambda_1$ and decreased background absorption intensity reflect the formation of Ni^{2+} complexes with the diamines and the dissolution of colloidal particles, respectively. Thus, these results suggest that the formation of complexes with TM-EDA did not proceed effectively, presumably because of the absence of N-H bonds in TM-EDA.

vii) Curve fitting to FT of k^3-weighted EXAFS spectra

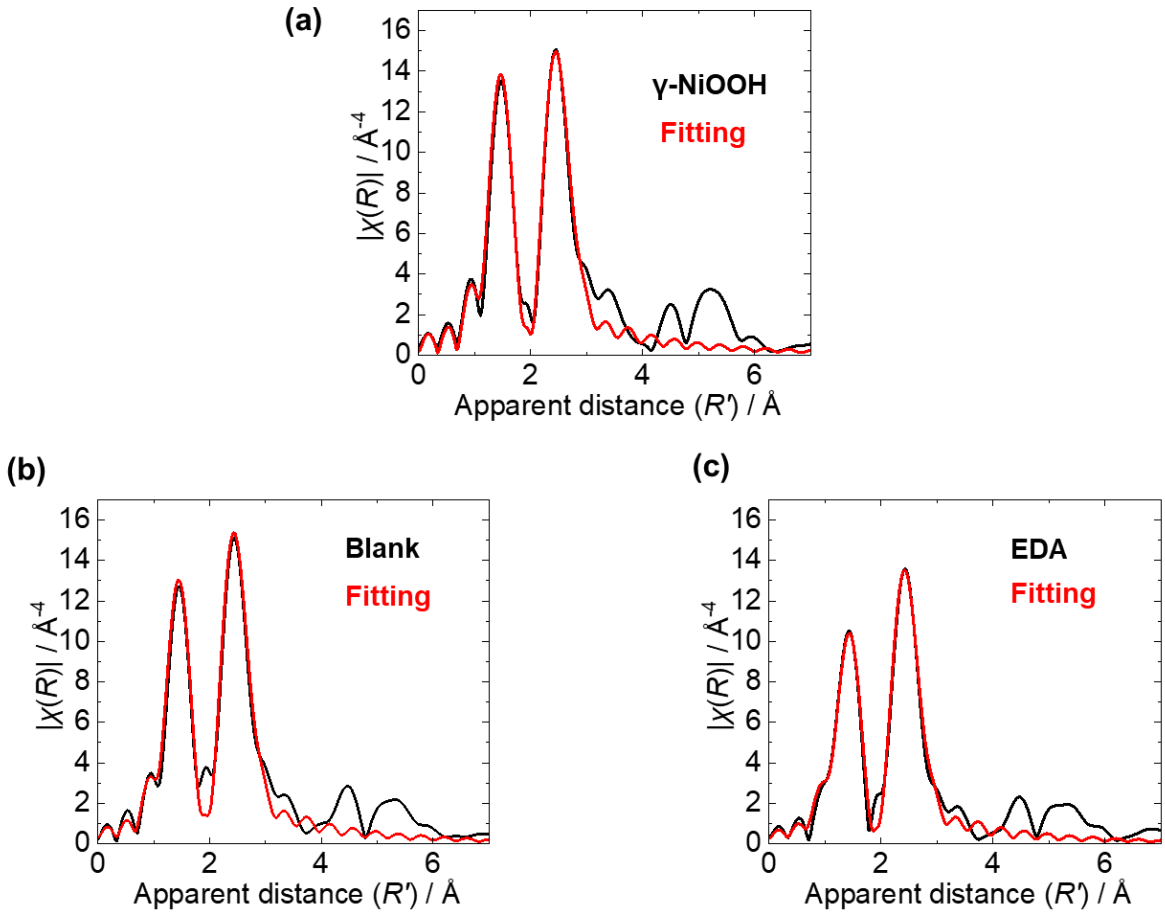

Figure S7. Curve fitting to FT of k^3-weighted EXAFS data for the (a) γ-NiOOH and (b) the Blank and (c) EDA Ni catalysts at 1.8 V vs. RHE in pH 11 K−P_i buffers (Fitting region: $1.0 \leq R \leq 2.8$ Å). The coordination number (N) and amplitude reduction factor (S_0^2) were fixed at 6 and 0.83, respectively.